

Spallation ultracold neutron production in superfluid helium

Y. Masuda¹, K. Hatanaka², S. Jeong¹, R. Matsumiya³, K. Matsuta³ and Y. Watanabe¹

¹*Institute of Particle and Nuclear Studies, High Energy Accelerator Research Organization, 1-1 Oho, Tsukuba, Ibaraki 305-0801, Japan*

²*Research Center for Nuclear Physics (RCNP), Osaka University, Ibaraki, Osaka 567-0047, Japan*

³*Graduate School of Science, Osaka University, 1-1 Machikaneyama, Toyonaka, Osaka 560-0043, Japan*

Neutrons of energies less than the Fermi potential of matter are defined as ultracold neutrons (UCN). UCN are completely reflected from a material surface, and then confined in a material bottle. Confined neutrons are very useful for the measurements of neutron electric dipole moment, neutron β decay. UCN are also useful for gravity, and neutron-antineutron oscillation experiments and so on. In these experiments, UCN density is one of the most important parameter. New generation UCN sources have been developed in many institutes, KEK, RCNP, Los Alamos, North Carolina, Indiana, SNS Oakridge, Grenoble, PSI and Munich, since the traditional UCN source like the turbine UCN source at Grenoble has limitations of UCN density because of Liouville's theorem.

We have been developing a new generation UCN source at RCNP, which breaks through the limitation. In 2002, we produced for the first time UCN in superfluid helium (He-II) placed in a spallation neutron source [1]. Neutrons in an energy region of MeV were produced upon spallation reactions in a lead target induced by a 400 MeV proton beam at RCNP. These neutrons were down scattered by deuterons in a neutron moderator complex of 300 K heavy water and 12 K heavy water, which was placed above the spallation target, to a cold neutron energy region. A He-II bottle was placed in the 12 K heavy water so that cold neutrons were down scattered by phonons in He-II to a UCN energy region. UCN produced upon the down scattering were extracted from the He-II to a vertical UCN guide, which was connected to the He-II bottle. UCN were guided to a UCN detector through a horizontal UCN guide and a gravity accelerator. The UCN density in the detector volume was 0.7 UCN/cm³ at a UCN maximum energy of 90 neV.

After this experiment, we have been improving the He-II spallation UCN source. The UCN density is represented in terms of a production rate and a storage time. The storage time is a UCN lifetime in a UCN bottle, which is denoted as τ_s . The production rate is obtained from a neutron flux Φ_n , a UCN production cross section $\sigma(E_{in} \rightarrow E < E_c)$ and a ⁴He nuclear number density N_{He} . The parameter E_{in} is an incident neutron energy, E a UCN energy and E_c is the Fermi potential of the He-II bottle. The UCN production cross section has a sharp peak at $E_{in} = 1$ meV like a δ function, where the neutron energy momentum dispersion curve intersects with the phonon dispersion curve, and then the production rate is represented as [2]

$$P(E) = \sigma_{coh}(E/E_{in}^*)^{1/2} \alpha S(k^*) N_{He} \Phi_n(E_{in}^*) \quad (1)$$

The parameter σ_{coh} is the ⁴He coherent scattering cross section, E_{in}^* the incident neutron energy at the intersection, k^* the neutron momentum at the intersection, the He-II form factor at the intersection, and $\alpha = 1.45$. The UCN density ρ_{ucn} is obtained from a double integration of the production rate over a proton beam impinging time and UCN energies E .

$$\begin{aligned} \rho_{ucn} &= \sigma_{coh}(E_{in}^*)^{-1/2} \alpha S(k^*) N_{He} \Phi_n(E_{in}^*) \tau_s [1 - \exp(-t_p/\tau_s)] \int_0^{E_c} E^{1/2} dE \\ &\cong 2/3 \sigma_{coh}(E_{in}^*)^{-1/2} \alpha S(k^*) N_{He} \Phi_n(E_{in}^*) \tau_s E_c^{3/2} \end{aligned} \quad (2)$$

Here, we assume proton beam impinging length (pulse width) t_p is longer than τ_s . As a result, the UCN density is proportional to the cold neutron flux Φ_n at 1 meV, the UCN storage time τ_s and the UCN momentum space volume factor $E_c^{3/2}$. The cold neutron flux is proportional to the proton beam current. The storage time depends on the He-II temperature and the wall conditions of the He-II bottle and the UCN guide.

Recently, we have improved the He-II cryostat, the He-II bottle and the UCN guide, which are shown in Fig. 1, for the increase in the UCN density. We have also placed a radiation shield in order to accept a higher proton beam current. We built a ³He circulation system for the operation of a ³He cryostat, which cools the He-II below 1 K. ³He gas is liquefied in a 1 K pot in a ⁴He cryostat and then transferred to a ³He pot in the ³He cryostat. The temperature of the ³He pot is lowered below 1 K by means of ³He pumping. A He-II pot is attached at the bottom of the ³He pot so that the He-II is cooled through a copper fin heat exchanger. The He-II pot connects with a He-II double tube through a He-II pipe. The He-II double tube connects with the He-II bottle, where UCN is produced, through a thin slit. We operated the improved He-II cryostat and then condensed ⁴He gas at the He-II pot until the level of He-II in the He-II bottle reached the upper part of the double tube. The temperature of the ³He pot was lowered to 0.7 K and then the temperature of the double tube become 0.8 K. The temperature of the He-II bottle was expected to be lower than 0.9 K.

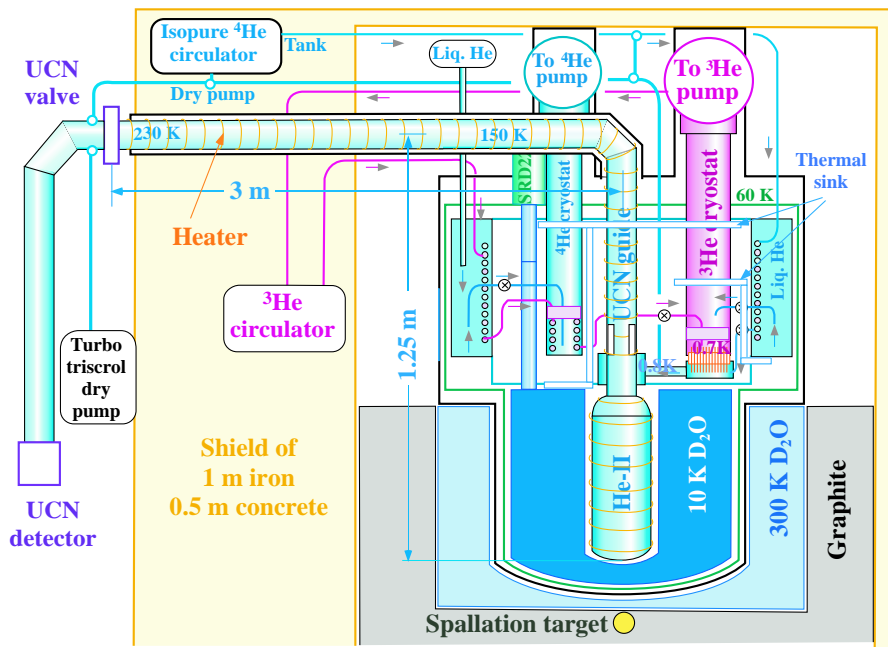


Figure 1: He-II spallation UCN source.

We have wound heaters on the outer surface of the He-II bottle and the UCN guide for baking in vacuum. After baking and before the operation of the He-II cryostat, we replaced hydrogen with deuterium on the inner surface of the He-II bottle and the UCN guide in order to decrease the UCN wall loss. We have also attached a UCN valve for UCN experiments.

We have placed a UCN detector of ^3He gas at the end of the gravity accelerator, and then switched on the proton beam. We have measured a pulse height spectrum obtained from a nuclear reaction, $n + ^3\text{He} \rightarrow p + t + 0.77 \text{ MeV}$. The result is shown in Fig. 2. The peak around channel 50 arose from full energy absorption. The steep rise around channel 10 arose mainly from electric noise. In Fig. 3, a time spectrum of UCN counts is shown for a 1 s of proton pulse. In a few seconds after switching off the proton beam, the UCN count reached the maximum, which arose from UCN diffusion from the He-II bottle to the UCN detector. At the detector, UCN were completely absorbed, therefore this process is a UCN emptying from the He-II bottle.

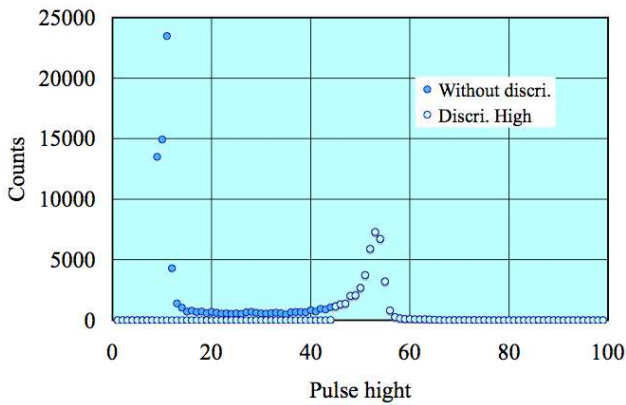


Figure 2: UCN pulse height spectrum.

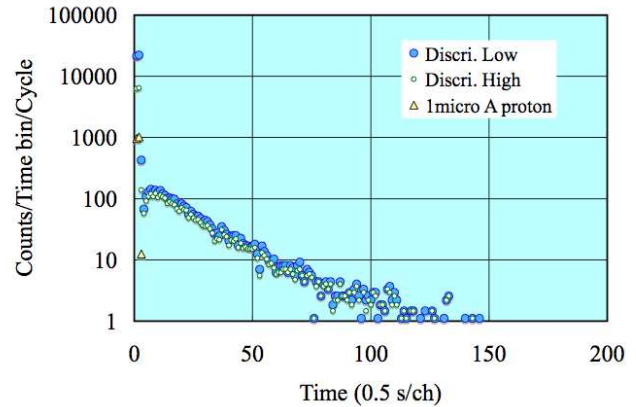


Figure 3: UCN production without the annular disk.

We placed an annular stainless steel disk in front of the UCN detector in order to avoid the complete loss at the detector. The diameter of the hole was 1 cm. UCN were partially lost at the UCN detector. Almost all UCN were reflected from the annular disk. The result of the UCN time spectrum is shown in Fig. 4. The rather slow rise time of the UCN counts after switching off the proton beam arises from longer UCN diffusion between the He-II bottle and the annular disk compared with the case without the annular disk. UCN go back and forth many times between the He-II bottle and the annular disk. The longer decay constant arises from

the partial loss at the detector.

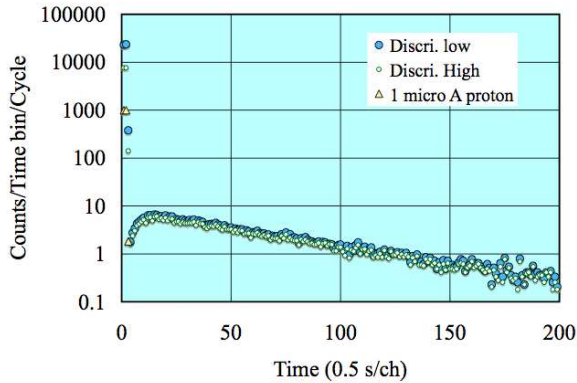


Figure 4: UCN production with the annular disk.

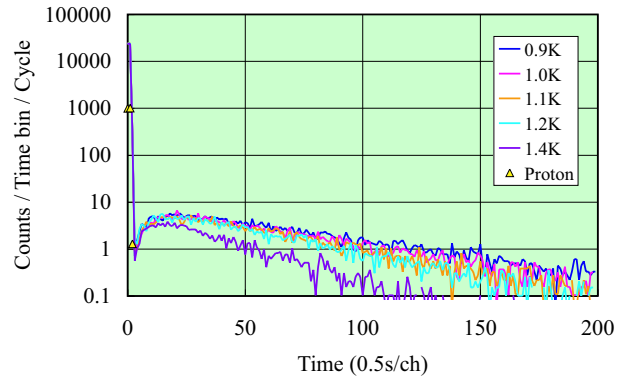


Figure 5: He-II temperature dependence.

We have inserted a 5 cm diameter UCN guide before the vertical UCN guide of 8.5 cm diameter. The diameter of the horizontal UCN guide is also 8.5 cm. We have also changed the temperature of the He-II bottle. In Fig. 5, the UCN time spectra at He-II temperatures of 0.9, 1.0, 1.1, 1.2 and 1.4 K in the double tube are shown. The rise time of the UCN counts become longer because of the smaller UCN flow rate through the narrow UCN guide. The decay constant did not change much at 0.9, 1.0, 1.1 and 1.2 K. At 1.4 K the decay constant become shorter than at other temperatures, but much longer than the proton pulse width 1s. The change in the value of $1 - \exp(-t_p/\tau_s)$ is only a few % between 0.9 and 1.4 K. The smaller peak count at 1.4 K around channel 10 may arise from UCN loss during diffusion.

We increased the proton pulse width from 1 to 60 s. The results are shown in Fig. 6 and Fig. 7. The effect of the proton pulse width on the UCN count is represented in terms of $1 - \exp(-t_p/\tau_s)$. The effect of different storage times at different He-II temperature on the UCN counts can be also discussed in terms of this factor. But, the difference in the UCN counts in Fig. 7 is not simply explained by the change in the UCN storage time. This may arise from the UCN loss during diffusion. The measurements mentioned above are denoted as open modes, because UCN valve was always opened. We also measured the time spectra with UCN valve operation. The UCN valve was closed when the proton beam was switched on, and then opened with a delay time when the proton beam was switched off. We changed the delay time. This measurement is denoted as a delay mode. The results of the UCN counts are shown in Fig. 8. The decay constant obtained from the delay mode measurement was consistent with the open mode measurement.

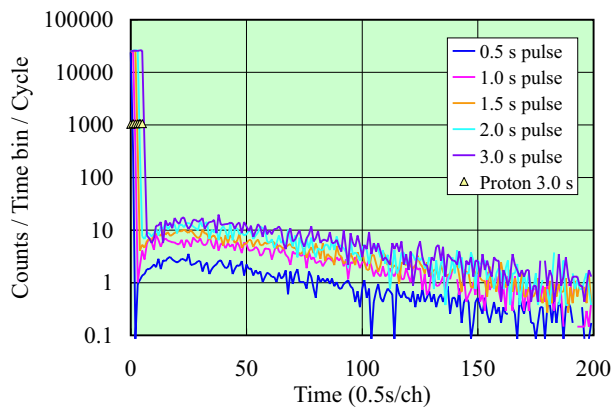


Figure 6: Proton pulse width dependence.

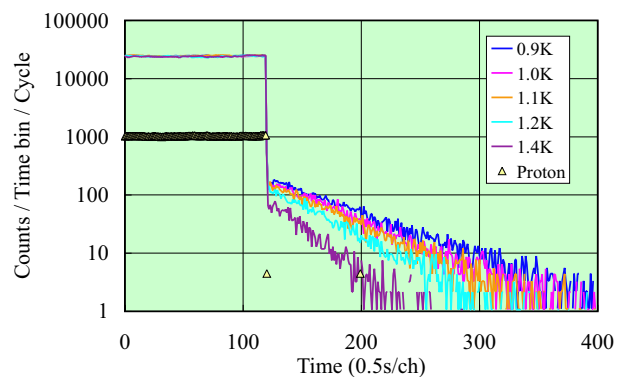


Figure 7: 60 s UCN production.

We reversed the UCN valve operation. The UCN valve was opened when the proton beam was switched on, and then closed when the proton beam was switched off. This measurement is denoted as a filling mode. We also measured the decay constant for the filling mode measurement. The result is shown in Fig. 9 as a function of the He-II temperature. No significant He-II temperature dependence was observed at 0.9, 1.0, 1.1 and 1.2 K. In the filling mode measurement, UCN lose arises from the wall collision and ^4He gas collision. The ^4He gas collision rate $1/\tau_{He}$ can be obtained from an equation

$$1/\tau_{He} = \rho\nu\sigma_s \quad (3)$$

in terms of ^4He nuclear number density ρ , ^4He velocity ν and the neutron cross section of ^4He σ_s . If we use the ideal gas equation and the relation $1/2 \cdot m_{\text{He}} \nu^2 = kT$ in order to obtain ρ , then the collision rate is obtained as

$$1/\tau_{\text{He}} = 0.047PT^{-1/2}s^{-1}. \quad (4)$$

Here, the parameter m_{He} is ^4He mass, k Boltzman constant and P ^4He gas pressure in Torr. We use the neutron cross section of 0.76 b for free ^4He . If we use the saturated vapor pressure of helium at 0.9, 1.0, 1.1 and 1.2 for P , and the temperature of the gravity accelerator for T , then the value of τ_{He} becomes very large. At the present condition, the storage time is limited by the loss rates at the wall collision and the detector. Therefore, no significant He-II temperature dependence was observed.

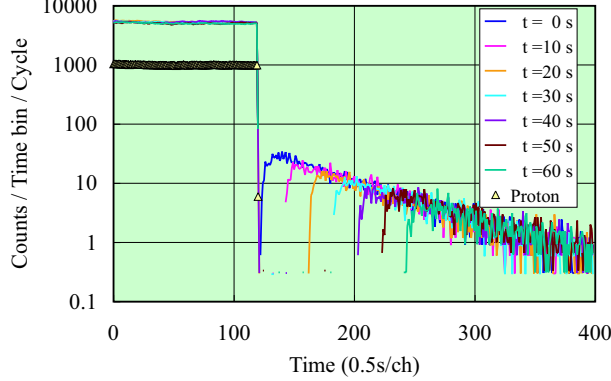


Figure 8: Delay mode measurement.

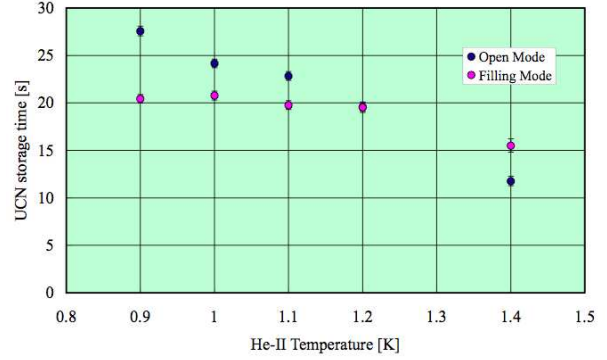


Figure 9: UCN storage time.

The He-II temperature dependence of the storage time at the open mode measurement is also shown in Fig. 9. In this mode, the storage time depends also on the loss rate at the horizontal and vertical UCN guides, and the He-II bottle. The effect of the UCN detector becomes smaller, because the volume for UCN storage becomes larger. The wall loss rate should be small after baking. The ^4He gas collision rate at the He-II temperature of 0.9 K is very small even at the low ^4He gas temperature. The He-II phonon collision rate is also very small at 0.9 K [3]. However, the observed storage time, which is 28 s at 0.9 K, is much shorter than expected. At higher He-II temperatures the storage times become smaller and smaller because of increases in ^4He saturated vapor pressure and He-II phonon number density. The storage time of 12 s at 1.4 K arises from these effects.

The rather short storage times at 0.9, 1.0, 1.1 and 1.2 K than expected may arise from a ^3He impurity in He-II. The neutron absorption rate of the ^3He impurity $1/\tau_{^3\text{He}}$ is obtained from the same equation as Eq. (3) in terms of a ^3He nuclear number density ρ , a neutron velocity ν , and the neutron absorption cross section of ^3He σ_a . Because the absorption cross section has the $1/\nu$ dependence, the absorption rate has no velocity dependence. The absorption cross section has a value of 5333 b at $\nu = 2200$ m/s. If we assume the ^3He impurity of the natural abundance 1.37×10^{-6} , then the absorption rate becomes $1/\tau_{^3\text{He}} = (28.4 \text{ ms})^{-1}$. We used distilled ^4He gas. The ^3He impurity is expected to be much smaller than the natural abundance. But, we need to decrease the ^3He impurity less than 10^{-10} so that we obtain a storage time of longer than 390 s. The present ^3He impurity may be not so small.

We estimated the UCN density in an experimental volume. The maximum UCN energy in the horizontal UCN guide is 90 neV, because the Fermi potential of the He-II bottle is 210 neV and the height of the horizontal UCN guide is 1.2 m. The average UCN velocity is 3.1 m/s, if we assume the statistical energy distribution. The UCN flow rate from the UCN valve, where experimental UCN bottles is attached, to the gravity accelerator is represented as $1/4 \cdot \rho_{\text{ucn}} \nu_{\text{av}} S$ in terms of the UCN density ρ_{ucn} , the average velocity ν_{av} and the cross section S at the horizontal UCN guide. The UCN count rate at the detector becomes $1/4 \cdot \rho_{\text{ucn}} \nu_{\text{av}} S \cdot S_h / S \cdot \varepsilon$. Here, S_h is the area of the detector window, which is $0.5^2 \pi \text{ cm}^2$, and ε detector efficiency, which is 0.68. The UCN density was obtained from the UCN count rate, which was 409 counts/s, to be 10 UCN/cm^3 . The UCN density of ILL is 50 UCN/cm^3 in the source volume of $E_c = 335 \text{ neV}$, but 0.7 UCN/cm^3 in the EDM cell of $E_c = 100 \text{ neV}$. Therefore, our present UCN density is the world's top class.

The present He-II temperature is rather high because of a higher heat load to He-II than expected. The higher heat load may arise from a He-II film flow. We need a window, for example a thin aluminum sheet in order to cut the film flow. We have checked the effect of the aluminum sheet on UCN. We removed the annular disk and placed a 100 mm aluminum sheet in front of the UCN detector, and then carried out the UCN production and detection with UCN valve operation. The UCN valve was closed and opened when the proton beam was switched on and off without delay time, respectively. The results of the UCN counts are shown

in Fig. 10. The effect of the aluminum sheet was very small, which was explained by attenuation at single transmission through the aluminum sheet. We placed again the annular disk and repeated the UCN production and detection. The results are also shown in Fig. 10. The attenuation of UCN counts when we placed the aluminum sheet become larger, because UCN go back and forth many times between the detector and the He-II bottle through the aluminum sheet after opening the UCN valve. The short UCN storage time arose from the same reason. But, if we fill a UCN experimental bottle with a filling time of less than 7 s, we can obtain 60% of UCN from the horizontal UCN guide through the aluminum sheet. If the filling time is longer, we will loose much UCN.

For further improvement in the UCN density, we are studying a horizontal UCN extraction from the He-II bottle as shown in Fig. 11. In this arrangement, we expect

1. larger effective volume of He-II for the UCN production,
2. higher E_c for extracted UCN,
3. more efficient UCN extraction and transport from the He-II bottle.

We will place the cryogenic window of thin aluminum. We will place a UCN valve before the cryogenic window in order to avoid the multiple transmission loss. The heat load from the H-II film flow will be reduced, and then He-II temperature will be lower. We will use ^4He gas with a negligibly small ^3He impurity, which was purified by using superfluid film flow [4]. We expect the cold neutron flux will increase by factor 5 by using a 5 μA proton beam, effective He-II volume factor 2, extraction and transport efficiency factor 2 and storage time factor 5. As a result we will obtain a UCN density of 1000 UCN/cm³ with the improved UCN source at RCNP.

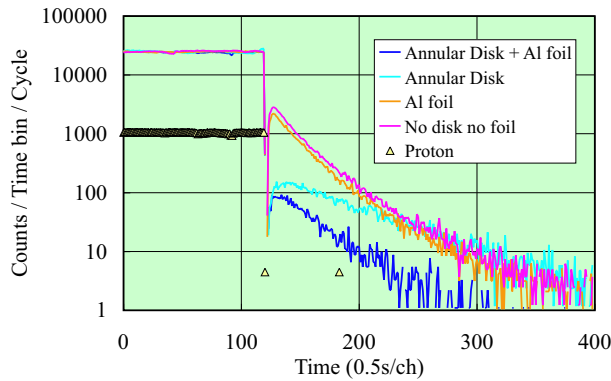


Figure 10: Effect of Al window.

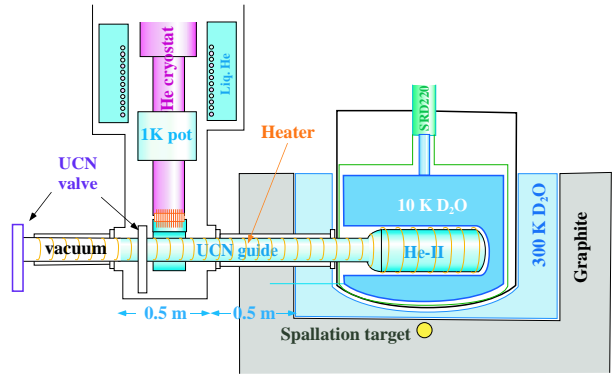


Figure 11: Horizontal UCN extraction.

References

- [1] Y. Masuda, T. Kitagaki, K. Hatanaka, M. Higuchi, S. Ishimoto, Y. Kiyonagi, K. Morimoto, S. Muto, and M. Yoshimura, Phys. Rev. Lett. 89 (2002) 284801.
- [2] R. Golub and J. Pendlebury, Phys. Lett. 62A (1977) 337.
- [3] R. Golub, C. Jewell, P. Ageron, W. Mampe, B. Heckel and I. Kilvington, Z. Phys. B51 (1983) 187.
- [4] We bought isotopically pure ^4He from Prof. P.V.E. McClintock, University of Lancaster.